Volume 16 | Number 7 | 21 February 2014 | Pages 1219–1396

CrystEngComm

www.rsc.org/crystengcomm

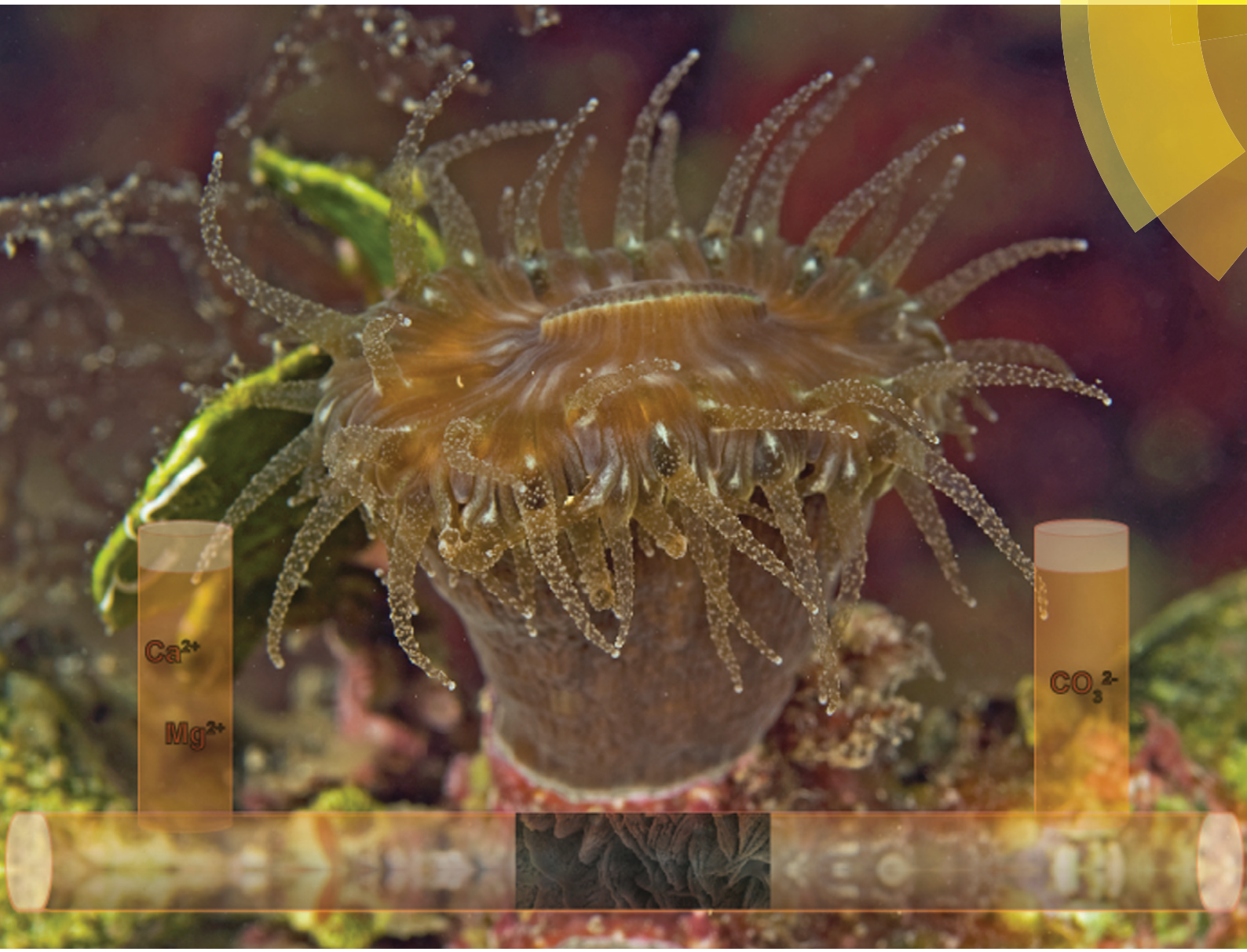

ROYAL SOCIETY OF CHEMISTRY

COVER ARTICLE

Gómez-Morales, Falini *et al.*

Exploring coral biomineralization in gelling environments by means of a counter diffusion system

CrystEngComm

PAPER

View Article Online
View Journal | View Issue

Exploring coral biomineralization in gelling environments by means of a counter diffusion system†

Cite this: *CrystEngComm*, 2014, **16**, 1257

M. Sancho-Tomás,[a] S. Fermani,[b] S. Goffredo,[c] Z. Dubinsky,[d] J. M. García-Ruiz,[a] J. Gómez-Morales*[a] and G. Falini*[b]

Received 18th September 2013,
Accepted 8th November 2013

DOI: 10.1039/c3ce41894d

www.rsc.org/crystengcomm

The crystallization of skeletal aragonite by corals takes place in sites whose physical characteristics resemble those of a highly viscous sol or a gel. In these sites, biomolecules are secreted by calicoblast cells of the coral and some of them become entrapped in the skeleton. To explore the biomineralization process, a series of calcium carbonate crystallization experiments were carried out in a counter-diffusion system (CDS) containing a viscous agarose sol with two dissolved intra-skeletal soluble organic matrices (SOM) that were extracted from *Balanophyllia europaea*, a zooxanthellate coral, and *Leptopsammia pruvoti*, an azooxanthellate species. The influence of the viscosity of the media and the presence of Mg^{2+} were investigated in two additional sets of experiments, one using an agarose gel of variable viscosity, and another allowing Mg^{2+} to diffuse from the cationic reservoir. The main findings are the following: (i) the species-specific molecular composition of the two SOMs has a different impact on the crystallization parameters and morphology of calcium carbonate; (ii) the viscosity of the gelling media, and thus its porosity, is important in regulating the SOM action; (iii) Mg^{2+} is important in defining specific and sharp limits of supersaturation under which crystallization occurs; (iv) the polymorph distribution is determined by SOM concentration. Thus, through the use of the CDS, it was possible to first study *in vitro* the biomineralization of zooxanthellate and azooxanthellate corals.

Introduction

Scleractinia corals represent the biggest source of biogenic calcium carbonate[1,2] on Earth and are among the fastest marine mineralizing organisms.[3] Despite their great contribution to oceanic biomineralization,[4] many aspects of their mechanism of mineralization are still a source of discussion and controversy. It has long been recognized that coral skeletons comprise both inorganic (aragonite) and organic components,[5,6] but the level of biological control over calcification is still an open issue. The scleractinian skeleton (Fig. 1) is composed of groups of needle-like aragonite crystals that radiate out from the *center of calcification*,[7] rich in calcium and sulphur.[8,9] This structural organization is controlled by specific macromolecules and is only slightly affected by external environmental parameters.

Coral mineralizes at the interface between the polyp's calicodermic tissue and the skeleton. This region is extremely rich in glycoproteins and glycosaminoglycans able to bond

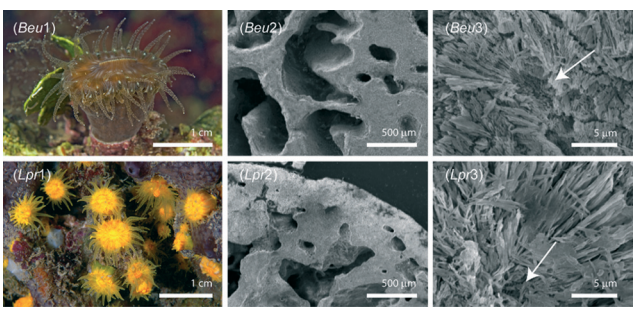

Fig. 1 Underwater *in situ* camera pictures of *B. europaea* (*Beu*1) and *L. pruvoti* (*Lpr*1). SEM cross section images of the skeleton of *B. europaea* (*Beu*2, 3) and *L. pruvoti* (*Lpr*2, 3) are also shown. In them, the different macroscale organization of the septa and microscale organization of the aragonitic fibers and of the *centers of calcification* are evident. The arrows indicate *centers of calcification* surrounded by aragonite fibers.

[a] *Laboratorio de Estudios Cristalográficos, IACT (CSIC-UGR), Avda. Las Palmeras, nº 4, E-18100 Armilla, Spain. E-mail: jaime@lec.csic.es*
[b] *Dipartimento di Chimica "G. Ciamician", Alma Mater Studiorum Università di Bologna, via Selmi 2, I-40126 Bologna, Italy. E-mail: giuseppe.falini@unibo.it*
[c] *Marine Science Group, Department of Biological, Geological and Environmental Sciences, Section of Biology, Alma Mater Studiorum University of Bologna, Via Selmi 3, 40126 Bologna, Italy*
[d] *The Mina and Everard Goodman Faculty of Life Sciences, Bar Ilan University, Ramat Gan, Israel*

† Electronic supplementary information (ESI) available: Optical microscope images, XRD patterns, FTIR spectra and low-magnification SEM pictures of calcium carbonate precipitates. See DOI: 10.1039/c3ce41894d

water molecules; thus the coral mineralization site was suggested to have the features of a highly viscous sol.[10] An amorphous organic membrane was observed between the calicodermis and the skeleton, and it was postulated that the site of mineralization is a colloidal gel matrix.[11]

Recent research suggested that there is a pathway involving direct seawater transport to the calcifying media in coral, which links the site of calcification to the surrounding ocean.[12] Other similar *in vivo* experiments showed that seawater acidification leads to a gradual relative decrease in pH of the medium in the calcification site, leading to an increasing pH difference between the calcification site and seawater.[13] The direct seawater transport to the calcification site implies that the precipitation of aragonite could be due to the high content of Mg^{2+} in seawater, with respect to calcium ions[14] (Mg/Ca molar ratio equal to 5). However, control of the local saturation state at the nucleation site requires the involvement of biological macromolecules, which are secreted by the calicoblast cells. The role of these macromolecules is also to control the structural and textural organization of the mineral regions of the skeleton. Moreover, their activity could be regulated by the presence of Mg^{2+}.[2–4] Goffredo *et al.*[15] showed that the intra-skeletal organic matrix from the Mediterranean solitary zooxanthellated coral *Balanophyllia europaea* favours the precipitation of aragonite and that this occurs through a transient phase of amorphous calcium carbonate stabilized by lipids. Furthermore, they showed that the organic matrix molecules also controlled the morphology of the precipitated calcium carbonate crystals. The influence of coral intra-skeletal organic matrix in the precipitation of calcium carbonate ($CaCO_3$) has also been demonstrated for the tropical species *Acropora digitifera*, *Lophelia pertusa* and *Montipora caliculata*.[16] This study highlighted the importance of the low molecular weight macromolecules in the control of calcium carbonate polymorphism. Important recent research has shown that four highly acidic proteins, derived from expression of genes obtained from the common stony coral, *Stylophora pistillata*, can spontaneously catalyse the precipitation of aragonite *in vitro* from seawater.[17] However, despite these advances, the chemical and physical processes that take place at the nucleation site are still only partly understood.

In the present study, the crystallization of calcium carbonate was carried out in a counter diffusion system (CDS)[18,19] using a highly viscous agarose sol or an agarose gel[20] in which the intra-crystalline soluble organic matrix (SOM) extracted from the solitary Mediterranean corals (Fig. 1) *B. europaea* (*Beu*SOM), zooxanthellate, and *L. pruvoti* (*Lpr*SOM), azooxanthellate, was added. These two species differ in the presence of symbiotic photosynthetic algae (zooxanthellae), which provide the main energetic support to corals that host them,[21,22] and are thought to facilitate calcification by raising the pH in their proximity. The CDS method[23,24] was proven to be a valid tool in the study of biomineralization processes,[25,26] allowing discrimination between inhibition/promotion of an additive on the nucleation/growth processes. The aim of the present study is to understand the influence of SOM in the precipitation of calcium carbonate in environments with different viscosities and to test the role of diffusing Mg^{2+}.

Results

Overview on SOM composition

The SOMs were characterized by their amino acid composition and by using FTIR spectroscopy (Fig. 2). The amino acid composition was in agreement with that observed in many intra-skeletal acidic macromolecules. It was characterized by a high content of aspartic (and asparagine) and glutamic (and glutamine) residues.

The carboxylate-bearing residues (*Asx* and *Glx*) represented the 52.0 and the 42.5 mol% of residues in *Beu*SOM and *Lpr*SOM, respectively; in the latter, a higher content of *Ser* and *Gly* (17.4 and 20.9) was present with respect to the former (12.9 and 17.8). The FTIR spectra showed that *Beu*SOM had, with respect to *Lpr*SOM, a lower absorption in the bands in zone 1 and a different structure of the bands in zone 3, which were due to methyl and methylene functional groups and glycosidic ether groups, respectively. The *Lpr*SOM also showed a stronger absorption in the bands at 1147 cm^{-1}, which could be attributed to the sulphate group.[27]

Calcium carbonate precipitation in the highly viscous sol by CDS

A reference experiment of calcium carbonate crystallization was carried out by diffusing, in the highly viscous agarose sol, a 0.5 M calcium chloride solution from the cationic reservoir and a 0.5 M sodium hydrogen carbonate solution from the anionic one. The measured parameters in the U-tube setup, as defined in the Experimental section, are the following: t_w (waiting time), x_o (starting point of precipitation) and Δ (crystal growing space). The first precipitate appeared after a t_w of 22 ± 8 h at x_o position equal to 0.62 ± 0.05. The precipitation evolved symmetrically with respect to x_o,

	Lpr	*Beu*
Asx**	33.1	46.4
Glx***	9.4	6.6
Ser	17.4	12.9
Gly	20.9	17.8
His	3.7	2.4
Thr	-*	0.3
Arg	-	0.5
Ala	6.8	4.1
Tyr	-	0.2
Cys	1.2	1.0
Val	2.9	2.6
Met	-	-
Phe	0.8	1.1
Ile	1.5	1.6
Leu	2.1	1.9
Lys	-	0.5

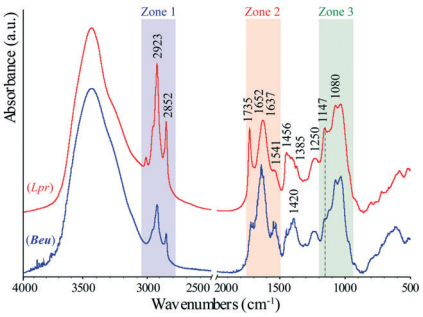

Fig. 2 Left, amino acid composition of the SOMs from *B. europaea* and *L. pruvoti*. The amino acid content is reported as mol percentage. Some amino acids were not detected and some chromatographic signal could not be assigned. For this reason, the sum of the amino acid percentages is lower than 100. Right, FTIR spectra from the SOMs from *B. europaea* (*Beu*) and *L. pruvoti* (*Lpr*). In the figure, three zones (1–3) are highlighted; they correspond to regions where the main absorption bands due to lipids, proteins and polysaccharides, respectively, are located. The dotted line indicates an absorption band typical of sulphate groups.

and after 14 days from the onset of the experiment, the Δ value was 0.30 ± 0.03 (Fig. 3; Table 1). Isolated particles were observed in the highly viscous sol under an optical microscope (Fig. 4A and S1A†), and they were identified as calcite using X-ray diffraction (Fig. S2†). Calcite appeared as crystals, 75 to 200 μm long, displaying rhombohedral {10.4} faces plus less developed {hk.0} faces (Fig. 5A), as already reported.[28,29]

Calcium carbonate precipitation in the highly viscous sol containing SOMs by CDS

The *Beu*SOM was added to the highly viscous sol at concentrations of 50 μg mL^{-1} (*c*) or 250 μg mL^{-1} (5*c*). Under these conditions, t_w was 32 ± 8 h and 52 ± 4 h and x_o was 0.66 ± 0.04 and 0.69 ± 0.05, respectively. The precipitation evolved asymmetrically with respect to x_o and roughly stopped in the position 0.60 ± 0.01 and 0.64 ± 0.02 in the cationic reservoir direction and in the position 0.70 ± 0.03 and 0.73 ± 0.02 in the anionic reservoir direction, using *Beu*SOM concentrations equal to *c* and 5*c*, respectively (Fig. 3; Table 1). The optical microscope pictures showed crystalline agglomerates of 100 to 400 μm, when *Beu*SOM *c* was used (Fig. 4D). Upon increasing the concentration of *Beu*SOM up to 5c, a continuum of particles whose sizes vary between 10 and 90 μm was observed (Fig. 4G). SEM images showed that these crystalline particles consisted of interconnected and prismatic-shaped nanoparticles, which formed a microscopically layered structure (Fig. 6B and D). When *Beu*SOM 5*c* was used, a little distortion of the layered structure and a rounding at the edges of the particles were observed, when compared to those obtained using *Beu*SOM *c*.

The dissolution of *Lpr*SOM at concentrations of 50 μg mL^{-1} (*c*) and 250 μg mL^{-1} (5*c*) into the highly viscous sol resulted in t_w values of 37 ± 15 h and 41 ± 16 h and x_o values of 0.65 ± 0.05 and 0.68 ± 0.03 for concentrations *c* and 5*c*, respectively. In both cases, the precipitation evolved symmetrically with respect to x_o. Under the optical microscope (Fig. 4J and M), the precipitates appeared to be formed by agglomerated particles. The increase in concentration of *Lpr*SOM from *c* to 5*c* caused a decrease in the size of the particles from 60–250 μm to 15–80 μm, respectively, and sharper borders of the crystallization space (Δ). The SEM images showed that the precipitates consisted of spherulitic particles (Fig. 7A and C; Fig. S4†) with a textural organization similar to that observed in the presence of *Beu*SOM *c* (Fig. 7B). Calcite was the only phase detected using X-ray powder diffraction (Fig. S2†).

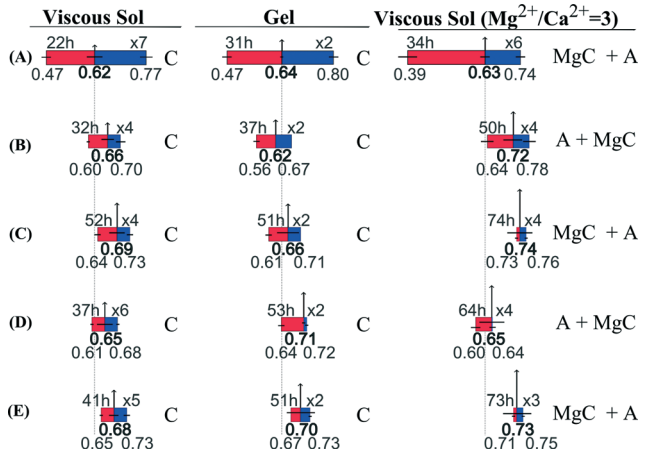

Fig. 3 Graphical representation of the measured parameters in the precipitation experiments of calcium carbonate carried out by CDS. In the absence (A) and in the presence of SOMs from *B. europaea*, at concentration *c* (B) and 5*c* (C), and from *L. pruvoti*, at concentration *c* (D) and 5*c* (E). The left column refers to the highly viscous sol experiments, the middle column to the gel experiments and the right column to the highly viscous sol experiments adding Mg^{2+} in the cation reservoir. The length of the tubes has been normalized from the cation reservoir (0) to the anion reservoir (1). The real length of the U-tubes was 45 mm. Red and blue colours indicate the crystallization region from the starting point of crystallization (x_o, bold numbers) to the cation reservoir (left-lower corner) and anion reservoir (right-lower corner), respectively. Arrows indicate the waiting time (t_w, hours, left-upper corner) and the number of replica is shown in the right-upper corner. Horizontal black lines in the middle of each figure and vertical grey lines on the arrow show the variability in the measurements. Phases were also indicated as calcite (C), Mg-calcite (MgC) and aragonite (A).

Calcium carbonate precipitation in the gel containing SOMs by CDS

These experiments were carried out to study the influence of the increased degree of entanglement of agarose molecules in the calcium carbonate precipitation process. Increasing agarose concentration from 0.1% (w/v) to 0.2% (w/v) resulted in longer t_w values (Table 1). When SOMs 5*c* were used, the position of x_o appeared closer to the anionic reservoir than in the pure gel reference experiment (Fig. 3). When *Beu*SOM *c* was added, x_o did not differ from the reference experiment, while a significant shift towards the anionic reservoir was observed using *Lpr*SOM *c*. The values of Δ and its evolution with time did not vary when using the gel instead of the highly viscous sol. Only when using *Lpr*SOM *c* did the precipitation evolve asymmetrically with respect to x_o (0.71 ± 0.01), with Δ being longer toward the cationic reservoir (0.64 ± 0.02) than toward the anionic one (0.72 ± 0.01).

Optical microscope pictures of Δ showed that in the gel, the differences observed among trials were enhanced with respect to the highly viscous sol (Fig. 4), especially in the presence of *Lpr*SOM. Particularly, sharper Δ borders were observed using SOMs 5*c*. The particles showed morphologies and size distributions similar to those observed in the highly viscous sol (Fig. 5, 6 and 7). Only when *Lpr*SOM 5*c* was used were smaller crystals (15–50 μm) observed (Fig. S4†). Calcite was the only phase detected using X-ray powder diffraction.

Calcium carbonate precipitation in highly viscous sol containing SOMs and diffusing Mg^{2+} by CDS

The addition of Mg^{2+} in the cationic reservoir (Mg/Ca molar ratio equal to 3) always led to an increase of t_w and a shift of x_o toward the anionic reservoir. Interestingly, in the presence

Table 1 Summary of data from precipitation experiments of calcium carbonate by CDS in the absence and in the presence of SOM from *B. europaea* or *L. pruvoti*, entrapped in highly viscous agarose sol or gel and in the presence of Mg^{2+} in the cationic reservoir. The precipitation parameters refer to measures of the mineral precipitated in the U-tube: starting point of precipitation (x_o); length of the region around x_o (Δ); and waiting time (t_w). The precipitate features refer to the minerals after removal from the agarose media

	Viscous sol					Gel					Viscous sol (Mg^{2+}/Ca^{2+} = 3)				
	Ref.	*Beu c*	*Beu 5c*	*Lpr c*	*Lpr 5c*	Ref.	*Beu c*	*Beu 5c*	*Lpr c*	*Lpr 5c*	Ref.	*Beu c*	*Beu 5c*	*Lpr c*	*Lpr 5c*
x_o[a]	0.62 (0.05)	0.66 (0.04)	0.69 (0.05)	0.65 (0.05)	0.68 (0.03)	0.64 (0.01)	0.62 (0.00)	0.66 (0.07)	0.71 (0.01)	0.70 (0.09)	0.63 (0.03)	0.72 (0.06)	0.74 (0.08)	0.65 (0.08)	0.73 (0.09)
t_w[b]	22 (8)	32 (8)	52 (4)	37 (15)	41 (16)	31 (10)	37 (9)	51 (10)	53 (3)	51 (10)	34 (11)	50 (15)	74 (31)	64 (57)	73 (51)
Δ	0.30 (0.03)	0.09 (0.03)	0.10 (0.03)	0.08 (0.02)	0.08 (0.02)	0.33 (0.00)	0.11 (0.03)	0.10 (0.02)	0.08 (0.01)	0.06 (0.01)	0.35 (0.04)	0.13 (0.02)	0.03 (0.01)	0.05 (0.02)	0.04 (0.01)
Phase[c]	C	C	C	C	C	C	C	C	C	C	MgC A	A MgC	MgC A	A MgC	MgC A
Shape[d]	*rhom.*	*r. ag.*	*sp. ag.*	*r. ag.*	*s. ag.*	*rhom.*	*r. ag.*	*s. ag.*	*r. ag.*	*sp. ag.*	*ac. sp.*	*sm. sp.*	*sm. s. sp. ag.*	*sm. sp. sp. ag.*	*sm. sp. sp. ag.*
Size[e]	75–200	100–400	10–90 300	60–250	15–80	80–150	100–500	80–400	100–300	15–50	80–150	80–150	30–350	100–300	20–300

[a] These values are normalized with respect to the length of the U-tube from the cation (0) to the anion reservoir (1). Their associated standard deviations are reported in parentheses. [b] The value of t_w is measured in hours. [c] Precipitated mineral phase: C, MgC and A indicate calcite, Mg-calcite and aragonite, respectively. [d] Shape of crystals observed using SEM: *rhom.* indicates modified rhombohedra; *r. ag.* indicates agglomerates of modified rhombohedra; *sp.* indicates spherulites; *ac. sp.* indicates acicular spherulites; *sm. sp.* indicates spherulites with smooth surface; *sp. ag.* indicates agglomerates of spherulites. [e] Size distribution of precipitates measured along the main axis (μm). All standard deviations are reported within parentheses.

of *Lpr*SOM *c*, the x_o value (0.65 ± 0.08) was similar to that obtained in the absence of Mg^{2+}. In the presence of diffusing Mg^{2+}, the length of Δ from x_o to the cationic reservoir was greater than that toward the anionic one (0.24 ± 0.06 and 0.11 ± 0.03, respectively). The Δ values were shorter than those observed in the Mg^{2+} free experiments (Fig. 3; Table 1).

In highly viscous sol, Mg^{2+} favoured the precipitation of large rounded and small peanut-shaped particles (Fig. 4C). The addition of SOMs brought about a reduction of crystallization density. Spherical and isolated particles were always observed when SOM *c* was used, while when using SOMs 5*c*, the particles were more aggregated, and sharp Δ borders were observed closer to the anionic reservoir (Fig. 4). In the latter condition, agglomerates in addition to small particles were obtained. The spherulites observed in the reference experiment were composed of hexagonal needle-shaped microcrystallites (Fig. 5F). Slight morphological changes were observed by adding *Beu*SOM or *Lpr*SOM, while the concentration effect of SOM was more relevant. Using SOM *c*, the size of the crystals was more homogeneous than that obtained using SOM 5*c* (Fig. S4†). This observation agrees with the crystal aggregation observed in optical microscope pictures

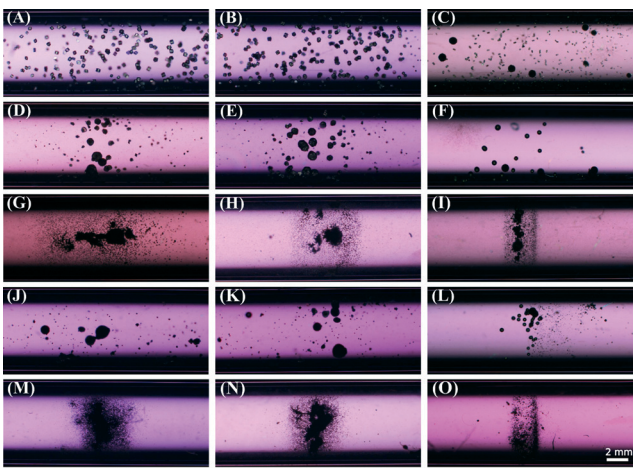

Fig. 4 Optical microscope images of crystal growing spaces (Δ) after 14 days, in the absence (A–C) and in the presence of SOMs from *B. europaea*, at concentration *c* (D–F) and 5*c* (G–I), and from *L. pruvoti*, at concentration *c* (J–L) and 5*c* (M–O). The left column refers to the highly viscous sol experiments, the middle column to the gel experiments and the right column to the highly viscous sol experiments, adding Mg^{2+} into the cation reservoir.

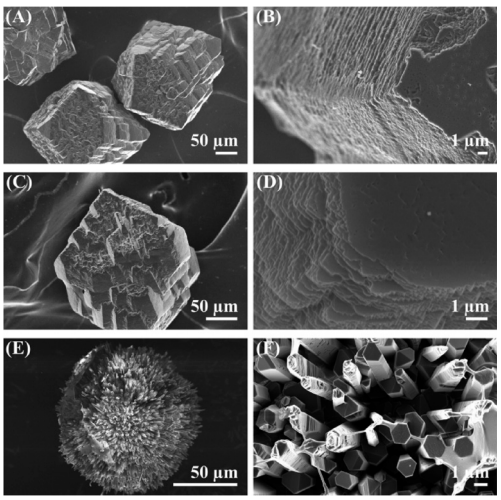

Fig. 5 SEM pictures showing the morphology of calcium carbonate crystals formed in highly viscous agarose sol in the absence of SOMs. The first row shows the $CaCO_3$ crystals grown in highly viscous agarose sol (A, B); the second row, in agarose gel (C, D); and the third row, in highly viscous agarose sol with the addition of Mg^{2+} into the cation reservoir (E, F). The columns show different magnifications. The morphology of precipitates did not allow us to distinguish between the two phases detected using XRD and FTIR analysis in the experiments carried out with added Mg^{2+}. These images are representative of the whole sample populations.

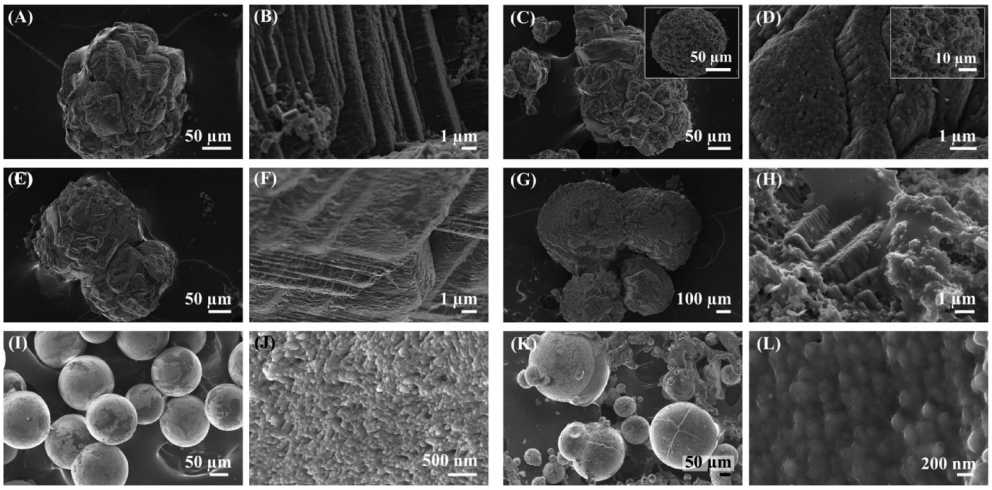

Fig. 6 SEM pictures showing the morphology of crystals formed in the presence of SOMs from *B. europaea*. The micrographs A, B, E, F, I and J show crystals obtained in the presence of *Beu*SOM *c*, whereas images C, D, G, H, K and L show crystals obtained in the presence of *Beu*SOM 5*c*. The first row (pictures A–D) corresponds to the highly viscous agarose sol experiments; the second row (E–H), to the agarose gel experiments and the third row (I–L), to the highly viscous agarose sol experiments with diffusing Mg^{2+}. The micrograph C and the inset show the two different morphologies of the precipitates formed in this condition. The inset of D is a high magnification of the spherulite shown in the inset of C. The observed morphologies of the precipitates obtained in the presence of Mg^{2+} (third row) did not allow us to distinguish between MgC and A, which were detected using XRD and FTIR analysis. These images are representative of the whole sample populations (Fig. S4†).

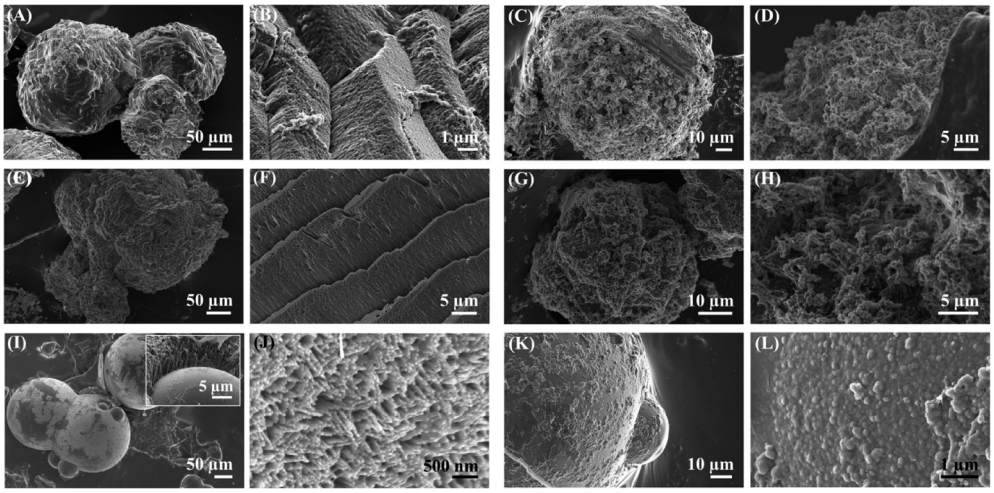

Fig. 7 SEM pictures showing the morphology of crystals formed in the presence of SOM from *L. pruvoti*. The micrographs A, B, E, F, I and J show crystals obtained in the presence of *Lpr*SOM *c*, whereas images C, D, G, H, K and L show crystals obtained in the presence of *Lpr*SOM 5*c*. The first row (pictures A–D) corresponds to the highly viscous agarose sol experiments; the second row (E–H), to the agarose gel experiments and the third row (I–L), to the highly viscous agarose sol experiments with diffusing Mg^{2+}. The inset in picture I shows a higher magnification of the peanut-like crystals. The observed morphologies of the precipitates obtained in the presence of Mg^{2+} (third row) did not allow us to distinguish between MgC and A, which were the phases detected using XRD and FTIR analysis. These images are representative of the whole sample populations (Fig. S4†).

(Fig. 4 and S1†). The presence of SOMs and diffusing Mg^{2+} made the prismatic crystals thinner, sharper and more co-oriented with respect to those obtained in the reference experiments. Using SOM 5c, spherulites displaying rough surfaces (Fig. 6L and 7L) were observed instead of the needle-shaped agglomerates. Aragonite and Mg-calcite were identified using X-ray diffraction and FTIR spectroscopy in all cases (Fig. S2 and S3†). The quantitative Mg-calcite/aragonite mass ratio (Fig. 8) was measured by analyzing the FTIR spectra. This ratio either increased or decreased with respect to the reference when SOM *c* or SOM 5*c* was used, respectively.

Discussion

Coral biomineralization occurs in a gel-like environment.[4] CDS has proven to be a valid tool to study the role of additives in nucleation/growth processes of calcium carbonate in such medium.[30,31] Thus, the use of the CDS in the presence

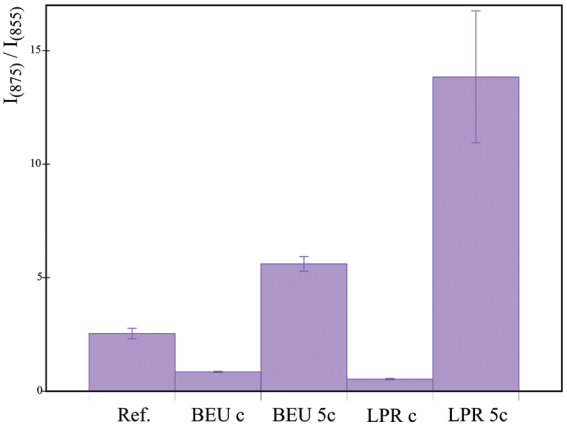

Fig. 8 Area ratios of the 875 cm^{-1} and the 855 cm^{-1} deconvoluted bands of precipitates. This area ratio represents a rough estimation of the Mg-calcite/aragonite mass ratio. The error bars were calculated by using the first-order Taylor method for propagating uncertainties considering the standard deviations associated with each area value.

of SOMs from the solitary Mediterranean coral *B. europaea* or *L. pruvoti* allows us to investigate differences and similarities in calcification between zooxanthellated and azooxanthellated species. To achieve this goal, a series of *in vitro* crystallization trials, with two concentrations of SOMs and different viscosity of the media and in the presence of diffusing Mg^{2+}, were carried out. In the reference experiments (*i.e.* the ones without SOMs entrapped in the highly viscous sol or gel), the first precipitates appeared in the same sites (x_o) situated in the vicinity of the anionic reservoir (Table 1). The x_o value must fulfil the equivalence rule,[17,22,30,31] and at this point, the ion activity product has to overcome the critical value needed to induce nucleation. x_o is displaced to the right of the U-tube (closer to the HCO_3^-/CO_3^{2-} reservoir) due to the much lower initial CO_3^{2-} concentration of this solution compared to that of Ca^{2+} ions.[30] The data also show that x_o is not affected by the degree of entanglement of the agarose molecules (*i.e.* no difference was observed between the highly viscous sol and the gel). This indicates that the diffusion rate of Ca^{2+} and carbonate species was equally affected by the different porosity of the two media. Interestingly, x_o values did not change in the experiments in the presence of Mg^{2+} (the concentration of Ca^{2+} was reduced to keep the ionic strength of the cationic reservoir solution constant). This apparent violation of the equivalence rule could be justified considering that Mg^{2+} can interact with CO_3^{2-} as Ca^{2+} does, although with less strength (the solubility of calcium carbonate is lower than that of magnesium carbonate). Thus, the activity of CO_3^{2-} interacting with Ca^{2+} is reduced proportionally to the Mg/Ca molar ratio, and the precipitation occurred in conditions as if the activity of CO_3^{2-} was lower. This hypothesis implies a longer t_w, as it was indeed observed. A contribution to the increase of t_w comes also from the inhibition of calcite growth due to the adsorption of Mg^{2+} on the calcite nuclei.[32,33] Diffusion of Mg^{2+} did not change significantly the Δ-values, but affected the symmetry of the growing front. The boundaries of the crystal growing spaces (Δ) represent the places where the activity of anions – in the zone close to the cationic reservoir – and the activity of cations – in the zone close to the anionic one – are the lowest to still sustain nucleation and growth of crystals. Here, it is shown that Mg^{2+} inhibits only the growth process, as indicated by the similar Δ-values.[30] Besides, Δ cannot be symmetric around x_o; in this case, the growing space starting from x_o up to the last observed crystals in the direction to the cationic reservoir was longer than that in the direction to the anionic one. This asymmetry suggests a different range of ionic activity of cations and anions to sustain nucleation and growth, and also could be a result of the lower activity of Ca^{2+} compared to that in the reference.

The addition of *Beu*SOM or *Lpr*SOM to the highly viscous sol, or the gel, increased the t_w and slightly shifted the x_o positions in the direction of the anionic reservoir. These effects were more marked when using the higher concentration of SOMs. The longer t_w with respect to the reference experiment most likely indicated an inhibition of the nucleation and/or incipient growth processes. Since in the presence of SOMs the Δ-values were shortened, an inhibition of the nucleation event was evident. Moreover, the morphology of the crystals was influenced by the presence of SOMs, suggesting that an inhibition of the growth process was present as well. The shift of x_o, which showed a trend, suggested that the presence of SOMs influenced the speciation of carbonate. Since *Lpr*SOM and *Beu*SOM contain acidic macromolecules characterized in their proteic regions by the presence of high amounts (almost 50 mol%) of aspartic and glutamic residues and glycosylated regions rich in sulphate groups, it can be supposed that their carboxylic group (pK_a around 4.5) could release protons in the highly viscous sol or in the gel, slightly reducing the activity of the carbonate ions in favour of that of hydrogen carbonate, but this was not observed in the presence of charged polypeptides.[30] On the other hand, it is also known that SOM is composed of intrinsically disordered proteins, IDPs.[34,35] The IDPs could locally change their ability to interact with diffusing ions due to their high structural flexibility. It is also noteworthy that SOMs also contain glycoproteins in which the pK_a, and therefore the ability to chelate calcium ions, changes with the degree of grafting.[36] Finally, the presence of lipids could also have an important role in stabilizing transient amorphous calcium carbonate forms.[15] Since SOMs are macromolecular mixtures, to specify a role for each organic component a further detailed study would be required.

We found that when increasing the degree of entanglement and the concentration of SOMs, the Δ borders became closer and sharper. Under these conditions, a lower ionic diffusion rate, a more confined space for the nucleation and growth of crystals and a higher SOM inhibition effect were present. The fact that the presence of Mg^{2+} made these borders even sharper suggested that Mg^{2+} could have a role in confining the crystallization conditions within defined calcium carbonate supersaturation values, as observed in the presence of *Beu*SOM or *Lpr*SOM.

In the presence of Mg^{2+}, the SOMs provoked a shift of x_o towards the anionic reservoir (as observed in the absence of Mg^{2+}), a longer t_w and co-precipitation of aragonite with Mg-calcite. Interestingly, the Mg-calcite/aragonite mass ratio was altered as a function of the concentration of SOMs; the low concentration (c) favoured the precipitation of aragonite while the high concentration ($5c$) favoured that of Mg-calcite (Fig. 8). This effect was more pronounced when using *Lpr*SOM. This Janus behaviour – the capability of the same family of molecules to promote and inhibit one phase – has been recently demonstrated for several additives in solution and in solid state.[37] Here, this behaviour can be justified in the context of the basic principles of biomineralization. Certain SOM molecules are able to interact with aragonite crystals, probably on specific crystalline planes. These molecules, when present in low concentration, can act as nucleation sites for aragonite and/or inhibition of calcite by Mg^{2+}, thus favouring aragonite precipitation. When the concentration is high, they are able to interact with the growing nuclei and/or enhance magnesium dehydration,[38] thus giving as a net result the inhibition of the precipitation of aragonite.

An intriguing effect of the interaction between Mg^{2+} and SOM was the nanoscale size of the crystals. The SEM images (Fig. 6L and 7L) show a granular structure when crystals grew in a highly viscous sol entrapping SOM, and Mg^{2+} ions were diffusing along the tube. This structure is very similar to that observed for corals by Falini *et al.*[16] in *in vitro* calcification experiments, by Vandermeulen and Watabe[39] and Motai *et al.*[40] in *in vivo* studies, as well as in biominerals from different phyla.[41,42] This granulated texture was identified as formed from amorphous calcium carbonate domains in sea urchin spicule[43] and cystoliths.[44] Pai and Pillai[45,46] proposed the formation of hollow triangular calcium carbonate forms from amorphous calcium carbonate spherical aggregates stabilized by the change in the conformation of a synthetic polypeptide induced by the presence of Mg^{2+}. These observations suggested a synergic role between SOMs and Mg^{2+}, which starts with a common amorphous precursor that later on transforms to aragonite or Mg-calcite depending on SOM concentration.

The stronger effect on crystallization parameters observed by the addition of *Lpr*SOM with respect to *Beu*SOM along with the higher impact on the crystal morphology cannot be justified only on the basis of the different amino acidic composition. Indeed, in several models of biomineralization, a more efficient role of acidic macromolecules, as calcium carbonate crystallization modifiers, has been related to a higher content of ionisable functional groups.[25,26,36,38,47,48] The used SOMs also differ in their glycosidic region structures and in the content of lipids. *Lpr*SOM has a higher degree of sulphonation along its glycosidic chains (Fig. 2, band at 1147 cm^{-1}) and presents a higher content of lipids. These two features entail an additional content of acidic functional groups compared to that due only to proteins. Sulphate groups in corals are mainly localized in the skeletal textural region referred to as *center of calcification*,[41] which represents the zone where the skeleton coral growth starts. Thus, in addition to the above proposed effects, the favoured precipitation of Mg-calcite in the presence of *Lpr*SOM could be also due to the different structure of the polysaccharide chains as well as to a reduced activity of Mg^{2+} in their presence.[49–52]

The diverse distribution of molecules in the two SOMs and their different impact on the precipitation of calcium carbonate could be related to the presence/absence of zooxanthella. It has already been shown that zooxanthellate and azooxanthellate corals differ in their average amino acidic composition, the latter being richer in acidic residues.[53] Here, it was observed that there are also differences in the content of lipids and in the structure and functionalization of polysaccharides. Zooxanthella provide energetic support to calcification through photosynthesis,[54] and it has been reported that they may influence the speciation of the inorganic carbon affecting the trafficking of protons around the nucleation site. Thus, it could be speculated that various molecular actors play different roles in the presence of photosynthesis in coral biomineralization.

Experimental

Coral skeletons

Samples of *Balanophyllia europaea* and *Leptopsammia pruvoti* were randomly collected during scuba diving in the North-Western Mediterranean Sea, at Calafuria 43°27′N, 10°21′E. *B. europaea* was collected at 6 m depth, *L. pruvoti* at 16 m depth. After collection, the corals were dipped in a sodium hypochlorite solution (commercial) for 4 days until the polyp tissue was completely dissolved, then the remaining skeletons were washed with double distilled water and dried in an oven at 37 °C for 24 h and stored. Each skeleton was analysed under a binocular microscope to remove fragments of substratum and calcareous deposits produced by other organisms. Successively, the skeletons were ground in a mortar to obtain a fine and homogeneous powder. The obtained powder was subsequently suspended (1% w/v) in a sodium hypochlorite solution (3% v/v) to remove traces of organic material not removed by the first treatment.

Extraction of the soluble organic matrix (SOM)

Five mL of milli-Q water, in which 2.5 g of powdered coral skeleton were dispersed, were poured into a 40 cm-long osmotic tube for dialysis (MWCO = 3.5 kDa; CelluSep®, MFPI). The sealed tube was placed into 1 L of 0.1 M CH_3COOH (Riedel de Haen) solution under stirring. The decalcification proceeded for 72 h. At the end, the tube containing the dissolved OM was dialysed against milli-Q water (resistivity of 18.2 MΩ cm at 25 °C; filtered through a 0.22 μm membrane) until the final pH was about 6. The obtained aqueous solution containing the OM was centrifuged at 30*g* for 5 minutes to separate the soluble (SOM) and the insoluble (IOM) OM fractions, which were then lyophilized and weighed.

Preparation of highly viscous agarose sol and gel

Firstly, an agarose stock solution of 0.3% (w/v) was heated up to 90 °C for 20 minutes to completely dissolve the agarose powder (Agarose D-5, Hispanagar). Then, the solution was cooled down (to about 40 °C) and thereafter mixed with the required volume of heated milli-Q water in different beakers partially submerged in a water bath at 50 °C to obtain final 0.1% or 0.2% (w/v) agarose solutions. In each beaker, a different amount of dissolved *Beu*SOM or *Lpr*SOM was added to reach a final concentration of 50 μg mL^{-1} (*c*) or 250 μg mL^{-1} (5*c*). The prepared solution was vortexed for 1 min and transferred to U-tubes using a 1 mL syringe.

Calcium carbonate precipitation by CDS

The experiments were carried out by using a U-tube system (Triana Science & Technology, S.L., Granada, Spain). These tubes have a column length of 45 mm, which is accessible to diffusing reagents from two side source reservoirs. To the cation reservoir, 0.2 mL of a 0.5 M solution with Mg/Ca ratio equal to 0 or 3 were added. These solutions were prepared by mixing $CaCl_2{\cdot}2H_2O$ and $MgCl_2{\cdot}6H_2O$ (Sigma-Aldrich). To the anion reservoir, 0.2 mL of 0.5 M $NaHCO_3$ solution (Fluka Biochemika) were added. The initial pH values of the solutions were: 5.7 for 0.5 M $CaCl_2$; 6.2 for 0.5 M $CaCl_2$–$MgCl_2$; and 8.1 for 0.5 M $NaHCO_3$. Cation and anion solutions counter-diffused through the column filled with a highly viscous agarose sol entrapping the SOMs. In the U-tube setup, we measured three main parameters: the waiting time (t_w) or time that elapsed from the onset of the experiment up to the appearance of the first precipitate (observed under an optical microscope at magnification 4×); the starting point of precipitation (x_o) or the distance from the cationic reservoir to the place where the first crystals appeared; and the crystal growing space (Δ) or the length within the column gel where precipitates were observed after 14 days from the onset of the experiment.[30] The pH values of the reservoirs did not change after the precipitation experiments. Precipitates were taken out from the tube and placed on top of a 0.45 μm pore size filter. The precipitates were washed several times with hot milli-Q water in order to remove agarose and then air-dried. All the experiments were performed at room temperature.

Characterization of $CaCO_3$ precipitates

Optical microscope (OM) observations were made using a Nikon AZ100 optical microscope connected to a digital camera (Nikon, DS-Fi1). Some samples were inspected using a Phenom™ scanning electron microscope (SEM). In addition, scanning electron micrographs of carbon-sputtered samples were collected using a GEMINI Carl Zeiss SMT field emission scanning electron microscope. The structural properties of the precipitates were analysed using X-ray diffraction (XRD) and Fourier transform infrared (FTIR) spectroscopy. Therefore, the crystals were ground and mounted on a Bruker X8 Proteum diffractometer equipped with a Microstar copper rotating anode generator, a κ goniometer, and a SMART 6000 CCD detector. The calculated XRD powder diffraction patterns were obtained after integrating the diffraction frames with the XRD2DSCAN.[55] Fourier transform infrared (FTIR) spectroscopy analyses were collected using a FTIR Nicolet 380 instrument (Thermo Electron Co.) from 4000 to 400 cm^{-1} at a resolution of 4 cm^{-1}. Disks were made by applying a pressure of 48.6 psi to a mixture consisting of 1 mg of sample and 100 mg of KBr by means of a hydraulic press. Mg-calcite to aragonite mass ratio semiquantitative analysis was performed integrating the deconvoluted bands at 875 cm^{-1} for calcite and at 855 cm^{-1} for aragonite. The error bars were calculated by using the first-order Taylor method for propagating uncertainties considering the standard deviation associated with each area value.[56]

Conclusions

Here, a study on $CaCO_3$ precipitation in highly viscous agarose sol and agarose gel hosting SOMs from two corals and diffusing Mg^{2+} is presented. The main results are the following: (i) the molecular composition of the two SOMs has a different impact on the crystallization parameters and morphology of $CaCO_3$; (ii) the viscosity of the gelling media, and thus its porosity, is important in regulating the SOM action; (iii) Mg^{2+} have a notable role in defining specific and sharp limits of supersaturation under which precipitation occurs as well as in phase selection; (iv) the phase distribution is affected by the SOM concentration. Thus, through the use of the CDS, it was possible to carry out a first study on *in vitro* biomineralization of a zooxanthellate and an azooxanthellate coral.

Abbreviations

$CaCO_3$	Calcium carbonate
Mg^{2+}, Ca^{2+} and CO_3^{2-}	Magnesium, calcium and carbonate ions
CDS	Counter-diffusion system
SOM	Soluble organic matrix
*Beu*SOM and *Lpr*SOM	Soluble organic matrix from *Balanophyllia europaea* and *Leptopsammia pruvoti*
c and 5*c*	Soluble organic matrix concentrations of 50 μg mL^{-1} and 250 μg mL^{-1}
t_w	Waiting time
x_o	Starting point of precipitation
Δ	Crystal growing space.

Acknowledgements

The research leading to these results has received funding from the European Research Council under the European Union's Seventh Framework Programme (FP7/2007-2013)/ERC grant agreement [no. 249930 – CoralWarm: Corals and global warming: the Mediterranean *versus* the Red Sea] and from Excellence project RNM5384 of Junta de Andalucía. M.S.T.

also thanks CSIC for her JAE-Pre research contract within the "Junta para la Ampliación de Estudios" co-funded by the European Social Fund (ESF). We deeply thank Gianni Neto for the coral underwater pictures. GF and SF thank the Consorzio Interuniversitario di Ricerca della Chimica dei Metalli nei Sistemi Biologici (CIRC MSB) for the support.

Notes and references

1 M. D. Spalding, C. Ravilious and E. P. Green, *World atlas of coral reefs*, Univ. of California Press, Berkeley, 2001.
2 A. L. Cohen and T. A. McConnaughey, *Rev. Mineral. Geochem.*, 2003, **54**, 151–187.
3 A. T. Marshall and P. Clode, *Coral Reefs*, 2004, **23**, 218–224.
4 S. Tambutté, M. Holcomb, C. Ferrier-Pagès, S. Reynaud, É. Tambutté, D. Zoccola and D. Allemand, *J. Exp. Mar. Biol. Ecol.*, 2011, **408**, 58–78, and references therein.
5 M. Wilfert and W. Peters, *Z. Morphol. Tiere*, 1969, **64**, 77–84.
6 S. D. Young, *Comp. Biochem. Physiol., Part B: Biochem. Mol. Biol.*, 1971, **40**, 113–120.
7 D. J. Barnes, *Science*, 1970, **170**, 1305–1308.
8 J. P. Cuif, Y. Dauphin, J. Doucet, M. Salome and J. Susini, *Geochim. Cosmochim. Acta*, 2003, **67**, 75–83.
9 J. P. Cuif and Y. Dauphin, *J. Struct. Biol.*, 2005, **150**, 319–331.
10 I. S. Johnston, *Int. Rev. Cytol.*, 1980, **67**, 171–214.
11 W. H. Bryan and D. Hill, *Proc. R. Soc. Queensl.*, 1941, **52**, 78–91.
12 A. C. Gagnon, J. F. Adkins and J. Erez, *Earth Planet. Sci. Lett.*, 2012, **329–330**, 150–161.
13 A. A. Venn, E. Tambutté, M. Holcomb, J. Laurent, D. Allemand and S. Tambutté, *Proc. Natl. Acad. Sci. U. S. A.*, 2012, **110**, 1634–1639.
14 L. Fernandez-Diaz, A. Putnis, M. Prieto and C. V. Putnis, *J. Sediment. Res.*, 1996, **66**, 482–491.
15 S. Goffredo, P. Vergni, M. Reggi, E. Caroselli, F. Sparla, O. Levy, Z. Dubinsky and G. Falini, *PLoS One*, 2011, **6**, e22338.
16 G. Falini, M. Reggi, S. Fermani, F. Sparla, S. Goffredo, Z. Dubinsky, O. Levi, Y. Dauphin and J. P. Cuif, *J. Struct. Biol.*, 2013, **183**, 226–238.
17 T. Mass, J. L. Drake, L. Haramaty, J. D. Kim, E. Zelzion, D. Bhattacharya and P. G. Falkowski, *Curr. Biol.*, 2013, **23**, 1126–1131.
18 H. K. Henisch and J. M. García-Ruiz, *J. Cryst. Growth*, 1986, **75**, 195–202.
19 M. Prieto, A. Putnis, L. Fernández-Díaz and S. López-Andrés, *J. Cryst. Growth*, 1994, **142**, 225–235.
20 A. Dey, G. de With and N. A. J. M. Sommerdijk, *Chem. Soc. Rev.*, 2010, **39**, 397–409.
21 D. Allemand, C. Ferrier-Pagès, P. Furla, F. Houlbrèque, S. Puverel, S. Reynaud, É. Tambutté, S. Tambutté and D. Zoccola, *C. R. Palevol*, 2004, **3**, 453–467.
22 M. F. Colombo-Pallotta, A. Rodríguez-Román and R. Iglesias-Prieto, *Coral Reefs*, 2010, **29**, 899–907.
23 J. M. García-Ruiz, *Key Eng. Mater.*, 1991, **58**, 87–106.
24 H. K. Henisch and J. M. García-Ruiz, *J. Cryst. Growth*, 1986, **75**, 203–211.
25 E. Asenath-Smith, H. Li, E. C. Keene, Z. W. Seh and L. A. Estroff, *Adv. Funct. Mater.*, 2012, **22**, 2891–2914.
26 J. R. Dorvee, A. L. Boskey and L. A. Estroff, *CrystEngComm*, 2012, **14**, 5681–5700.
27 F. S. Parker, *Applications of infrared, Raman, and resonance Raman spectroscopy in biochemistry*, Springer, New York, 1983.
28 H. Li, H. L. Xin, D. A. Muller and L. A. Estroff, *Science*, 2009, **326**, 1244–1247.
29 H. Li and L. A. Estroff, *CrystEngComm*, 2007, **9**, 1153–1155.
30 M. Sancho-Tomás, S. Fermani, M. A. Durán-Olivencia, F. Otálora, J. Gómez-Morales, G. Falini and J. M. García-Ruiz, *Cryst. Growth Des.*, 2013, **13**, 3884–3891.
31 L. A. Estroff, L. Addadi, S. Weiner and A. D. Hamilton, *Org. Biomol. Chem.*, 2004, **2**, 137–141.
32 F. Lippmann, *Sedimentary Carbonate Minerals: Minerals, Rocks and Inorganic Materials*, Springer-Verlag, Berlin, 1973.
33 G. Falini, S. Fermani, G. Tosi and E. Dinelli, *Cryst. Growth Des.*, 2009, **9**, 2065–2072.
34 A. Adamiano, S. Bonacchi, N. Calonghi, D. Fabbri, G. Falini, S. Fermani, D. Genovese, D. Kralj, M. Montalti, B. Njegić Džakula, L. Prodi and G. Sartor, *Chem.–Eur. J.*, 2012, **18**, 14367–14374.
35 M. Wojtas, P. Dobryszycki and A. Ożyhar, in *Advanced topics in biomineralization*, ed. J. Seto, InTech, 2012, ch. 1, pp. 1–32, and references therein.
36 D. Malferrari, S. Fermani, P. Galletti, M. Goisis, E. Tagliavini and G. Falini, *Langmuir*, 2013, **29**, 1938–1947.
37 J. Ihli, Y. Y. Kim, E. H. Noel and F. C. Meldrum, *Adv. Funct. Mater.*, 2013, **23**, 1575–1585.
38 S. Albeck, J. Aizenberg, L. Addadi and S. Weiner, *J. Am. Chem. Soc.*, 1993, **115**, 11691–11697.
39 J. H. Vandermeulen and N. Watabe, *Mar. Biol.*, 1973, **23**, 47–57.
40 S. Motai, T. Nagai, K. Sowa, T. Watanabe, N. Sakamoto, H. Yurimoto and J. Kawano, *J. Struct. Biol.*, 2012, **180**, 389–393.
41 J. P. Cuif, Y. Dauphin, B. Farre, G. Nehrke, J. Nouet and M. Salomé, *Mineral. Mag.*, 2008, **72**, 233–237.
42 J. H. E. Cartwright, A. G. Checa, J. D. Gale, D. Gebauer and C. I. Sainz-Díaz, *Angew. Chem., Int. Ed.*, 2012, **51**, 11960–11970.
43 Y. Politi, R. A. Metzler, M. Abrecht, B. Gilbert, F. H. Wilt, I. Sagi, L. Addadi, S. Weiner and P. U. P. A. Gilbert, *Proc. Natl. Acad. Sci. U. S. A.*, 2008, **105**, 17362–17366.
44 A. Gal, W. Habraken, D. Gur, P. Fratzl, S. Weiner and L. Addadi, *Angew. Chem.*, 2013, **125**, 4967–4970.
45 R. K. Pai and S. Pillai, *Cryst. Growth Des.*, 2007, **7**, 215–217.
46 R. K. Pai and S. Pillai, *J. Am. Chem. Soc.*, 2008, **130**, 13074–13078.
47 J. L. Arias and M. S. Fernández, *Chem. Rev.*, 2008, **108**, 4475–4482.
48 C. C. Tester, R. E. Brock, C. H. Wu, M. R. Krejci, S. Weigand and D. Joester, *CrystEngComm*, 2011, **13**, 3975–3978.
49 S. Weiner and L. Addadi, *Annu. Rev. Mater. Res.*, 2011, **41**, 21–40.

50 A. J. Giuffre, L. M. Hamm, N. Han, J. J. De Yoreo and P. M. Dove, *Proc. Natl. Acad. Sci. U. S. A.*, 2013, **110**, 9261–9266.
51 A. E. Stephenson, J. J. DeYoreo, L. Wu, K. J. Wu, J. Hoyer and P. M. Dove, *Science*, 2008, **322**, 724–727.
52 J. Tao, D. Zhou, Z. Zhang, X. Xu and R. Tang, *Proc. Natl. Acad. Sci. U. S. A.*, 2009, **106**, 22096–22101.
53 J. P. Cuif, Y. Dauphin, A. Freiwald, P. Gautret and H. Zibrowius, *Comp. Biochem. Physiol., Part A: Mol. Integr. Physiol.*, 1999, **123**, 269–278.
54 P. L. Jokiel, *Bull. Mar. Sci.*, 2011, **87**, 639–657.
55 A. Rodriguez-Navarro, *J. Appl. Crystallogr.*, 2006, **39**, 905–909.
56 S. Mekid and D. Vaja, *Measurement*, 2008, **41**, 600–609.

